Journal of Thermal Analysis and Calorimetry
https://doi.org/10.1007/s10973-026-15358-x

Enhancement of heat transfer and hydrodynamic performance in a double tube heat exchanger using transverse and helical turbulators with nanofluid

Ebrahim Tavousi[1] · Noel Perera[1] · Mostafizur Rahman[1] · Reaz Hasan[1] · Dominic Flynn[2]

Received: 19 October 2025 / Accepted: 25 January 2026

Abstract
Double tube heat exchangers (DTHEs) are widely used in industrial thermal systems, where improving heat transfer efficiency is critical for energy savings. This numerical study investigates the thermal–hydraulic performance of transverse and helical turbulator inserts with different rib geometries (rectangular, triangular, oval, and trapezoidal) used in combination with a water-based SiO_2 nanofluid in a counterflow DTHE. Steady-state laminar simulations were performed in ANSYS Fluent for Reynolds numbers between 400 and 2000. The results show that helical turbulators significantly outperform transverse designs, with the triangular helical turbulator achieving up to a 565% increase in the Nusselt number compared to pure water without inserts, while transverse trapezoidal turbulators reached a maximum enhancement of 470%. Owing to enhanced swirl generation and boundary-layer disruption, helical turbulators also yielded superior thermal–hydraulic performance, achieving a maximum performance evaluation criterion (PEC) of 3.17, compared to 1.9 for transverse configurations. These findings demonstrate the effectiveness of helical turbulator designs combined with nanofluids for improving DTHE performance in laminar-flow industrial applications.

Keywords Double tube heat exchanger · Nanofluid · Turbulator insertion · Heat transfer coefficient · Nusselt number · Thermal efficiency · Pressure drop

Introduction

Fossil fuels continue to supply approximately 84% of the world's energy, and with the increasing global energy demand, efficient thermal systems, such as heat exchangers, remain critical components in applications ranging from oil and gas processing to solar thermal systems [1, 2]. The rising demand for energy, driven by urbanization and population growth, exacerbates environmental concerns, particularly global warming. To mitigate these effects, improving energy efficiency and adopting renewable energy are crucial [3]. A key focus is on enhancing the efficiency of double tube heat exchangers (DTHEs), which are essential in various industries. By improving the thermal efficiency of DTHEs, we can achieve significant energy savings and cost reductions [4]. A DTHE consists of two concentric tubes. In this setup, one fluid flows through the inner tube, while another fluid moves through the space between the inner and outer tubes. This arrangement allows for efficient heat transfer between the fluids. The DTHE is widely used in industrial settings because it is simple, reliable, and effective in thermal exchange processes [5]. DTHEs are widely used in applications such as waste heat recovery, geothermal energy, combustion, latent heat energy storage, and air conditioning as well as in industries like chemical, food, oil, gas, pharmaceutical, and solar energy [2, 6]. Enhancing the performance of DTHEs can be approached through three main methods: active, passive, and combined methods [7]. Active methods use external power sources, such as vibration [8, 9], electric fields, ultrasonic vibration, mechanical aids, or magnetic fields, to increase heat transfer [10–12]. In contrast, passive methods improve heat transfer without external power, relying instead on extended surfaces and other design elements

✉ Noel Perera
Noel.Perera@bcu.ac.uk

[1] Department of Engineering, School of Architecture, Built Environment, Computing and Engineering, Birmingham City University, Birmingham B4 7XG, UK

[2] Vehicle Efficiency, Jaguar Land Rover, Gaydon CV35 0BJ, UK

Published online: 14 February 2026

[13–15]. Combined methods integrate both active and passive techniques for a synergistic effect [16, 17].

The passive heat transfer method can be divided into five main categories, as classified by Tavousi et al. [18]: turbulator insertion [19–21], increased surface area using fins [22], changes in geometry [23], the use of nanofluids [24–26], and combinations of these techniques [27]. A statistical analysis of more than 100 studies on these methods showed that combining turbulator insertion with nanofluids results in the highest increase in heat transfer rates [18]. A nanofluid is a fluid that contains particles of nanometer size suspended within it. Nanofluids, which consist of these nanoparticles dispersed in liquids, enhance the thermal convective and conductive heat transfer properties of the base fluids [28, 29]. The effects of nanofluids on heat transfer and fluid flow characteristics have been extensively investigated in recent studies, including applications such as magnetic hybrid nanofluids (Fe_3O_4/TiO_2) in turbulent regimes, pulsating nanofluid jet impingement, the influence of nanofluids on the optimization of turbulator hole diameters in geothermal heat exchangers, and the impact of nanoparticle size and pulsating flow on thermal performance [30–33].

Eiamsa-Ard et al. [34] conducted an experimental study on heat transfer in a circular tube with air flow under turbulent conditions and uniform wall heat flux, using full-length and short-length twisted-tape inserts (LR = 0.29–1.0). The full-length tape achieved the highest Nusselt number and friction factor, while short tapes showed up to 14% and 21% lower values, respectively. Correlations were developed for Nusselt number and friction factor across Reynolds numbers from 4,000 to 20,000. Saedodin et al. [35] performed a numerical study to examine how the geometry of a corrugated DTHE, specifically one with a heated inner tube, affects its efficiency. Their results showed that the highest thermal performance, with a value of 1.82, was achieved at a Reynolds number of 400 when using spiral fins. Gunes et al. [36] conducted an experimental study to evaluate the effects of different coil characteristics and Reynolds numbers on a coiled wire. Their findings indicated that inserting the coiled wire improved both the heat transfer rate and pressure drop. They concluded that this method is most effective at low Reynolds numbers. Noorbakhsh et al. [37] conducted a numerical analysis to assess the effect of adding twisted tapes within a double-pipe heat exchanger (DPHE). Their results showed that using a single twisted tape led to a 3.1% increase in the Nusselt number compared to using four twisted tapes. Ibrahim [38] carried out experimental studies to explore the impact of helical insert geometrical parameters on heat transfer enhancement in laminar flow within a horizontal flat tube. The findings demonstrated that reducing the spacer length and twist ratio led to increases in both the average friction factor and the Nusselt number. Nakhchi and Esfahani [39] conducted a numerical study to examine the impact of inserting perforated conical rings into a tube within a heat exchanger (HE) on thermal performance and flow dynamics. Their findings showed improvements in heat transfer and a reduction in pressure loss as a result of the perforated conical rings. In a separate experimental study, Sheikholeslami and Ganji [40] enhanced heat transfer in a DPHE by using perforated turbulators in the annulus section, achieving a peak performance evaluation criterion of 1.59 at a Reynolds number of 6000. Kumar et al. [41] conducted experimental research to investigate the impact of strip inserts within a DTHE using Fe_3O_4 nanofluid. They explored various concentrations of Fe_3O_4 nanofluid at different Reynolds numbers and strip aspect ratios to assess their effects on pressure drop, heat transfer rate, and overall effectiveness. The results indicated that the Nusselt number increased with higher Reynolds numbers and nanofluid concentrations, while it decreased with larger strip aspect ratios. In a related parametric study, Hangi et al. [42] sought to identify the optimal configuration for a DTHE, employing four types of helical strips on the annulus side and a helical insert on the tube side with nanofluid flow. Their findings revealed that heat transfer enhancement was further improved when nanoparticles were uniformly distributed, particularly in cases with higher mixing.

Hussein et al. [43] investigated the hydrothermal performance of a DTHE by examining different fin configurations and in-line arrangements, focusing on longitudinal, wavy, and split fins under comparable boundary conditions. Using 3D numerical modeling, they analyzed key parameters such as Nusselt number, friction factor, and thermal resistance and showed that wavy and split–wavy fins significantly enhanced heat transfer, with Model D achieving up to 46.39% higher Nu compared to the conventional model. In a related study, Azizi et al. [44] explored the turbulent hydrothermal characteristics of a DTHE equipped with twisted elliptical tubes, considering both uniform and non-uniform twist pitches and varying aspect ratios. Their results revealed that reduced twist pitch and increased aspect ratio induced stronger secondary flows, thereby augmenting heat transfer, while the counterflow configuration generally provided higher performance evaluation criterion values than parallel flow. Collectively, these studies highlight the role of internal geometry modifications, whether fin arrangements or twisted elliptical tubes, in enhancing heat transfer at the cost of higher pressure drop, providing valuable insights for optimizing DTHE design.

While the combination of turbulator insertion and nanofluids has demonstrated significant heat transfer enhancement [18], there remains a notable gap in research specifically focused on applying this technique within DTHEs. This study aims to address this gap by introducing newly designed helical and transverse turbulator inserts with distinct rib shapes, triangular, rectangular, trapezoidal, and oval, used

in conjunction with SiO_2 nanofluid. The transverse turbulator configuration was investigated in a previously published study by the authors (Tavousi et al. [20]) and is employed here solely for comparison with the proposed helical turbulator designs. The primary objective was to evaluate the impact of these innovative turbulator designs on heat transfer and fluid flow characteristics within a DTHE and identify the configuration that achieves the highest heat transfer enhancement. Additionally, the study examined the effects of varying turbulator heights and conducted a comparative analysis between helical and transverse turbulators to better understand their influence on hydrothermal properties under laminar-flow conditions within a Reynolds number range of 400 to 2000. This research makes a novel contribution to the field by providing valuable insights into optimizing DTHE performance through the integration of advanced turbulator designs and nanofluids.

Numerical setup

The dimensions of the DTHE include an inner copper tube with a diameter of 0.014 m and a wall thickness of 0.001 m and an outer tube with a diameter of 0.08 m. Both tubes have a length of 1.8 m. Turbulator insertions are introduced to enhance the heat exchange efficiency by disrupting the flow, thereby decreasing the thermal boundary layer near to the wall and enhancing the thermal mixing. These insertions are categorized into transverse and helical types, with shapes including rectangular, triangular, oval, and trapezoidal configurations. The dimensions of the turbulators, specifically, the distances between the ribs (s), the height of the ribs (h), and the width of the ribs (w), are critical parameters that were systematically varied to study their impact on the heat transfer and fluid flow within the DTHE. The diameter of the turbulator insertions is consistently maintained at 0.002 m, with the first rib positioned 0.01 m from the inlet, ensuring a uniform start point for comparing the results of different cases. Figure 1 depicts the geometry of the DTHE, both with and without the insertion of transverse turbulators. A 2D axisymmetric model was used for the transverse configuration due to its geometric symmetry around the axis. For the simulations of helical turbulator insertion, the same DTHE with the same dimensions was used to ensure comparable results. As with the transverse turbulators, four different shapes of helical turbulators were designed: rectangular, triangular, oval, and trapezoidal. Since the helical turbulator lacks symmetry, the entire DTHE was modeled in 3D for simulations. The helical twist ratio for all cases was set at 1 to 0.04 m, meaning one revolution of the helix is 40 mm. Additionally, the height of the helical turbulators (h) was varied to study its impact on the performance of the DTHE. The CFD simulations employed a coupled approach for velocity–pressure coupling, along with a second-order upwind scheme for the momentum and energy equations, based on the finite volume method. Figure 2 illustrates the configuration of helical turbulator insertions within the inner tube of the DTHE. Hot water and cold nanofluid were introduced through velocity inlets in the outer and inner tubes, respectively, and exited through pressure outlets. The copper wall separating the two flows was modeled as thermally coupled, allowing heat transfer between the inner and outer fluids. The outer wall of the outer tube was defined as a stationary adiabatic wall.

Table 1 presents the dimensionless parameters S, W, and H, derived from Eq. 15 in the Governing equations section, based on the selected dimensions of s, w, and h. The same aspect ratio was used to standardize the comparison and ensure fair evaluation across different turbulator types. The inner tube contained cold nanofluids at a constant inlet temperature of 295 K, while the outer tube was supplied with hot water at a constant inlet temperature of 335 K.

These temperature settings were chosen to reflect common industrial standards, ensuring the findings are relevant to practical applications [45–47]. Given that previous studies have shown that a single-phase approach compared to two-phase approach and the assumption of constant thermophysical properties yield results consistent with experimental data, these methods were adopted for the numerical analysis in this study [48, 49]. The assumption of constant thermophysical properties for the nanofluids was applied, with results showing less than a 2% deviation when compared to variable thermophysical properties. The flow was considered laminar in both the inner and outer tubes, with the outer tube maintaining a Reynolds number of 800 and the inner tube operating over a Reynolds number range of 400 to 2000, increasing by 400 at each step. The nanofluid used in the inner tube was SiO_2, at a 0.05 volume fraction. SiO_2 was selected based on our previous findings showing the highest heat transfer enhancement, its limited investigation with turbulator insertions, and its widespread, cost-effective use in industry [20, 50–52]. Detailed thermophysical properties of the materials used are provided in Table 2. Al_2O_3 was used in the validation section, while the thermophysical properties of copper were used for modeling heat transfer through the inner tube wall.

Governing equations

This study examines the heat transfer characteristics and fluid dynamics of laminar flow in a DTHE. The governing equations for steady-state laminar flow, including continuity, momentum, and energy equations, are expressed as follows. These equations provide a comprehensive

Fig. 1 Schematic of the analyzed DTHE, both with and without transverse turbulator inserts (not to scale)

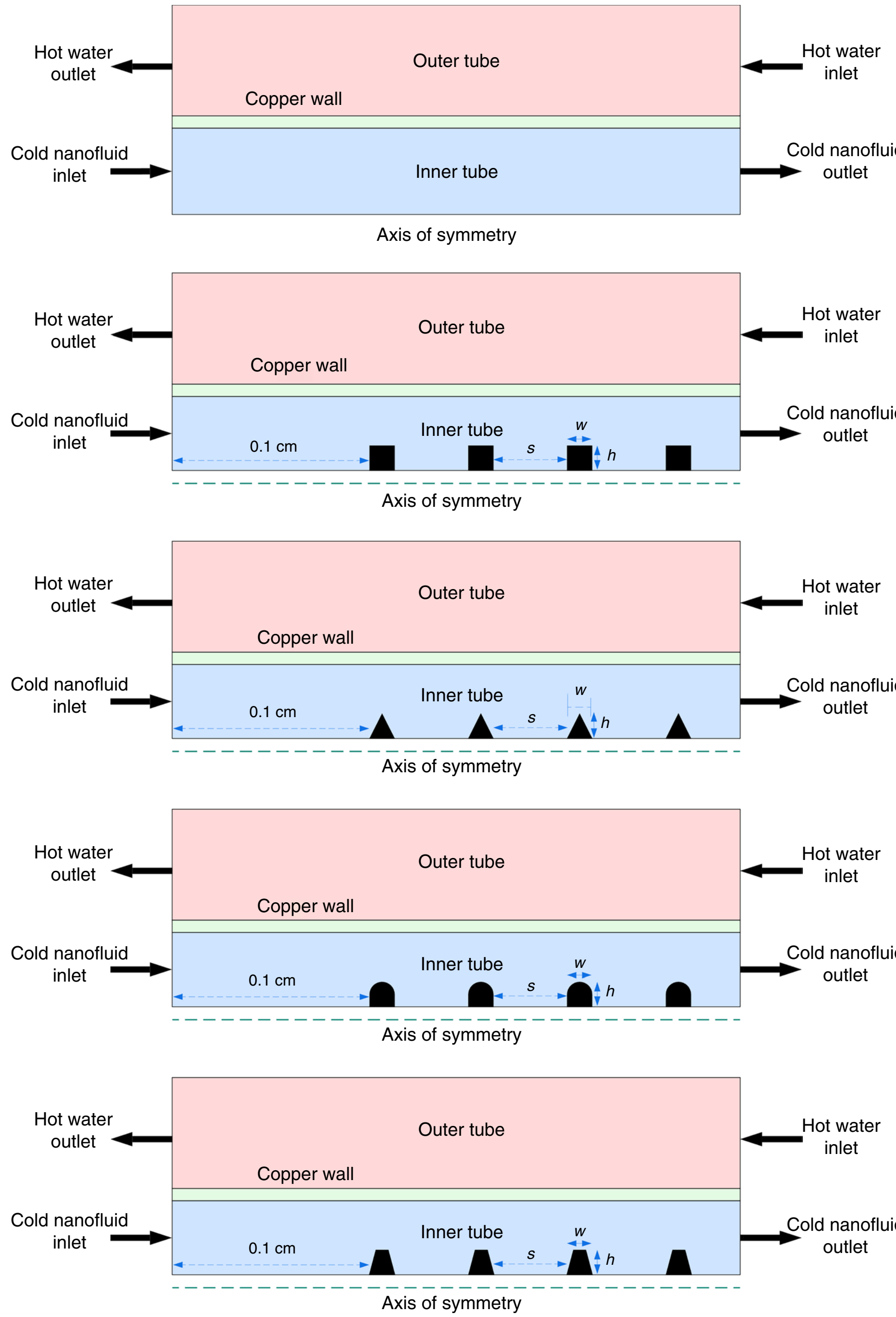

framework for analyzing and predicting the performance of DTHE under steady-state, laminar-flow conditions [56].

For steady, incompressible flow, the continuity equation is represented as:

$$\frac{\partial u}{\partial x} + \frac{\partial v}{\partial y} + \frac{\partial w}{\partial z} = 0 \tag{1}$$

The momentum equation for incompressible flow with constant viscosity is given by:

$$\nabla.(\rho VV) = -\nabla P + \nabla.(\mu \nabla V) \tag{2}$$

For incompressible flow with constant thermal conductivity, the energy equation is written as:

$$\nabla.\left(\rho V C_{\mathrm{p}} T\right) = \nabla.(k \nabla T) \tag{3}$$

Here, ρ denotes density, C_{p} represents specific heat, and k indicates thermal conductivity.

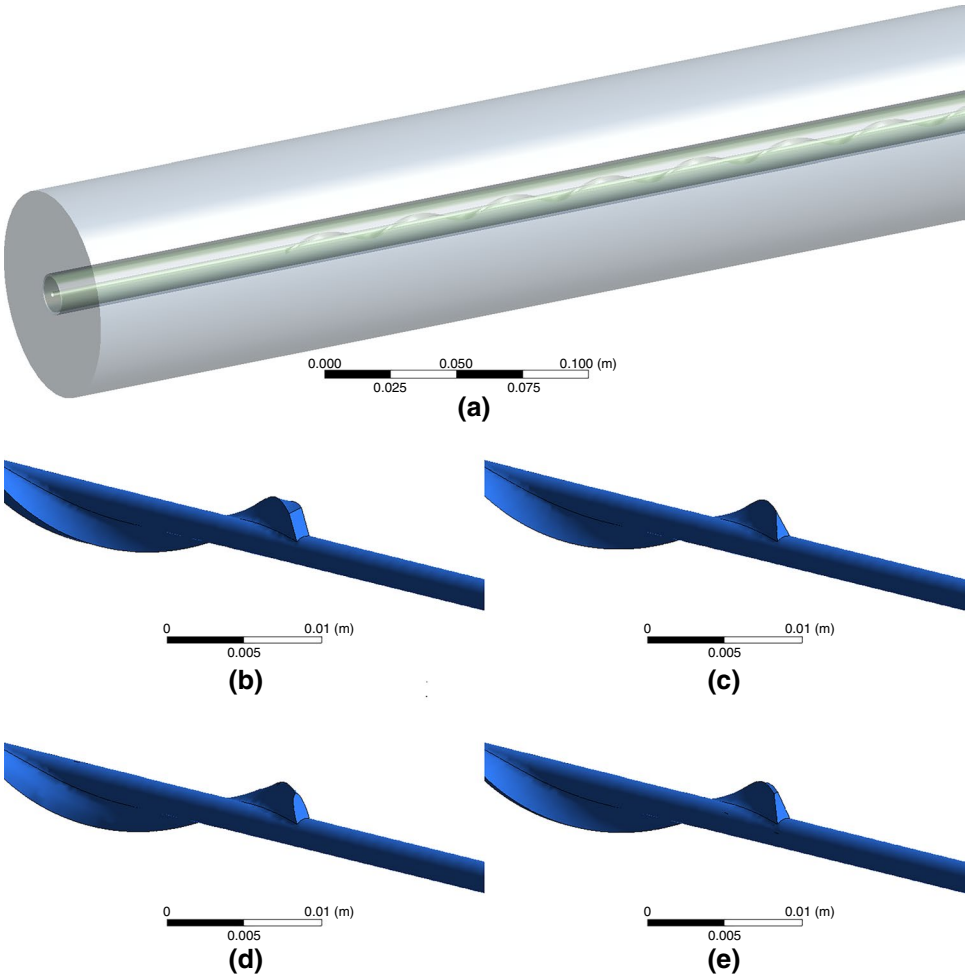

Fig. 2 Schematic of the analyzed DTHE, **a** overall domain and helical turbulators, **b** rectangular, **c** triangular, **d** oval, **e** trapezoidal

Table 1 Dimensionless key parameter values

s/m	*S*	*w*/m	*W*	*h*/m	*H*
0.02	2.86	0.001	0.14	0.001	0.14
0.04	5.71	0.002	0.29	0.002	0.29
0.06	8.57	0.003	0.43	0.003	0.43
0.08	11.43	0.004	0.57	0.004	0.57
0.10	14.29	0.005	0.71	0.005	0.71

Table 2 Thermophysical properties of the materials used in this study (nanoparticles with a size of 40 nm)

Thermophysical properties	Water [53]	Al_2O_3 [54]	SiO_2 [54]	Copper [55]
ρ/kg m^{-3}	997	3600	2200	8978
C_p/J kg^{-1} K^{-1}	4179	765	703	381
k/W m^{-1} K^{-1}	0.613	36	1.2	387.6
μ/N s m^{-2}	0.000855	–	–	–

The water-based SiO_2 was modeled using a single-phase approach, assuming uniform nanoparticle distribution, no slip between phases, and constant thermophysical properties. Nanoparticles are uniformly dispersed without agglomeration, sedimentation, or Brownian motion effects, and thermophysical properties are calculated based on volume fraction, temperature, and particle size using empirical correlations. The density and specific heat capacity of the nanofluid were determined based on the nanoparticle volume fraction [57–59]. The thermal conductivity and viscosity were calculated using the correlations proposed by Vajjha [60] and Sharma [61], respectively. These equations consider the effects of temperature, nanoparticle size, and volume fraction, resulting in predictions closely matching experimental data. The nanofluid properties were obtained using the following equations:

$$\rho_{nf} = (1-\varphi)\rho_b + \varphi\rho_p \tag{4}$$

$$(C_p)_{nf} = (1-\varphi)(C_p)_b + \varphi(C_p)_p \tag{5}$$

$$\frac{\mu_{nf}}{\mu_b} = \left(1+\frac{\varphi}{100}\right)^{11.3} \times \left(1+\frac{T_{nf}}{70}\right)^{-0.038} \times \left(1+\frac{d_p}{170}\right)^{-0.061} \tag{6}$$

$$\frac{k_{nf}}{k_b} = \left[\frac{k_p + 2k_b - 2(k_b - k_p)\varphi}{k_p + 2k_b + (k_b - k_p)\varphi}\right] \times 5\times 10^4 \beta\varphi\rho_b C_{p,b}\sqrt{\frac{\kappa T}{\rho_p d_p}} f(T,\varphi) \tag{7}$$

$$f(T,\varphi) = \left(2.8217\times 10^{-2}\varphi + 3.917\times 10^{-3}\right)\left(\frac{T}{T_0}\right) + \left(-3.0669\times 10^{-2}\varphi - 3.91123\times 10^{-3}\right) \tag{8}$$

The subscripts p, nf, and b represent particles, nanofluid, and base fluid, respectively.

The overall convection heat transfer coefficients and the Nusselt number for nanofluids flowing inside a tube with an inner radius of R_{in} can be calculated using the following equations [62, 63]:

$$\overline{h_{nf}} = \frac{1}{L}\int_0^L h_{nf}.dx_{|r=R_{in}} \tag{9}$$

$$\overline{Nu_{nf}} = \frac{\overline{h_{nf}}(2R_{in})}{k_{in}} \tag{10}$$

The subscript in indicates the inner tube, and L represents the tube length.

The empirical correlation for the Nusselt number in laminar-flow conditions for both the inner and outer tubes is expressed as follows [64]:

$$\mathrm{Nu} = 1.86\left(\mathrm{RePr}\frac{d}{L}\right)^{0.33} \tag{11}$$

Here, Re denotes the Reynolds number, Pr represents the Prandtl number, d is the tube diameter, and L is the length of the DTHE.

The pressure drop along a tube of length L is calculated using the following equation [65]:

$$\Delta P = \frac{fL\rho V^2}{2d_h} \tag{12}$$

where f is the friction factor, L is the DTHE length, ρ is the fluid density, and d_h represents the hydraulic diameter of the tube cross section.

The performance evaluation criterion (PEC) of the DTHE can be calculated using the following equation [66]:

$$\mathrm{PEC} = \frac{\left(\frac{\mathrm{Nu}}{\mathrm{Nu}_0}\right)}{\left(\frac{f}{f_0}\right)^{1/3}} \tag{13}$$

The subscript 0 denotes the base fluid without nanoparticles. In this study, the reference condition corresponds to pure water without turbulator insertion.

The relative error e_r can be determined using the following equation:

$$e_r = \frac{|\varepsilon - \hat{\varepsilon}|}{\hat{\varepsilon}} \times 100 \tag{14}$$

where ε represents the target parameter, and $\hat{\varepsilon}$ indicates the target parameter at the highest number of mesh elements.

The dimensionless key parameters for s, w, and h are defined by the following expressions:

$$S = \frac{s}{R_i}$$
$$W = \frac{w}{R_i} \tag{15}$$
$$H = \frac{h}{R_i}$$

Here, R_i is the radius of the inner tube.

Grid test and validation

Grid independence

To ensure the accuracy and reliability of computational simulations, a grid independence test was performed in this study, focusing on both transverse and three-dimensional (3D) helical turbulator insertions. The primary aim of this test was to verify that the numerical results remain stable and unaffected by variations in the computational grid size. Achieving grid independence is essential for validating the simulation outcomes, as it identifies the optimal grid size that balances computational efficiency with precision in the simulation results, thereby optimizing both time and cost. To this end, the mesh configuration was carefully designed to be denser near the walls and around the turbulators. This approach is critical, considering that these areas exhibit complex heat transfer and fluid flow behavior, necessitating increased resolution to accurately capture the phenomena. Figures 3 and 4 illustrate schematic diagrams of a grid with rectangular rib for a case of transverse turbulators and

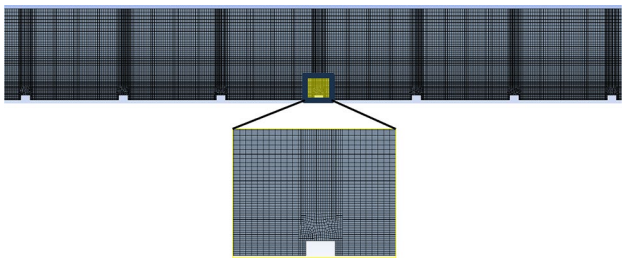

Fig. 3 Schematic of the overall domain with a mesh grid featuring a rectangular transverse turbulator

an oval helical turbulator for a case of helical turbulators, respectively.

The impact of varying mesh densities on heat transfer and hydrodynamic parameters was evaluated for both transverse and helical turbulator insertions. This assessment aimed to confirm the adequacy of mesh refinement and ensure independence within the computational simulations. The mesh independence test was evaluated based on three critical parameters: outlet temperature, pressure drop, and the average Nusselt number across the inner tube. Figure 5 illustrates that the optimal mesh comprises approximately 107,000 elements, with a maximum discrepancy of less than 2.2% compared to simulations employing the highest mesh density. Furthermore, Fig. 6 presents the variation in outlet temperature, pressure drop, and Nusselt number for the inner tube equipped with a rectangular helical turbulator. It shows that the deviation in outcomes with the use of 7,000,000 elements, as compared to the case with the highest number of elements, is less than 2%. To optimize computational time and expenses, the simulations utilized mesh sizes of approximately 107,000 for transverse turbulator insertions and about 7,000,000 elements for helical turbulator insertions. It was also concluded that the Nusselt number exhibited greater sensitivity to variations in the number of mesh elements relative to the other considered parameters.

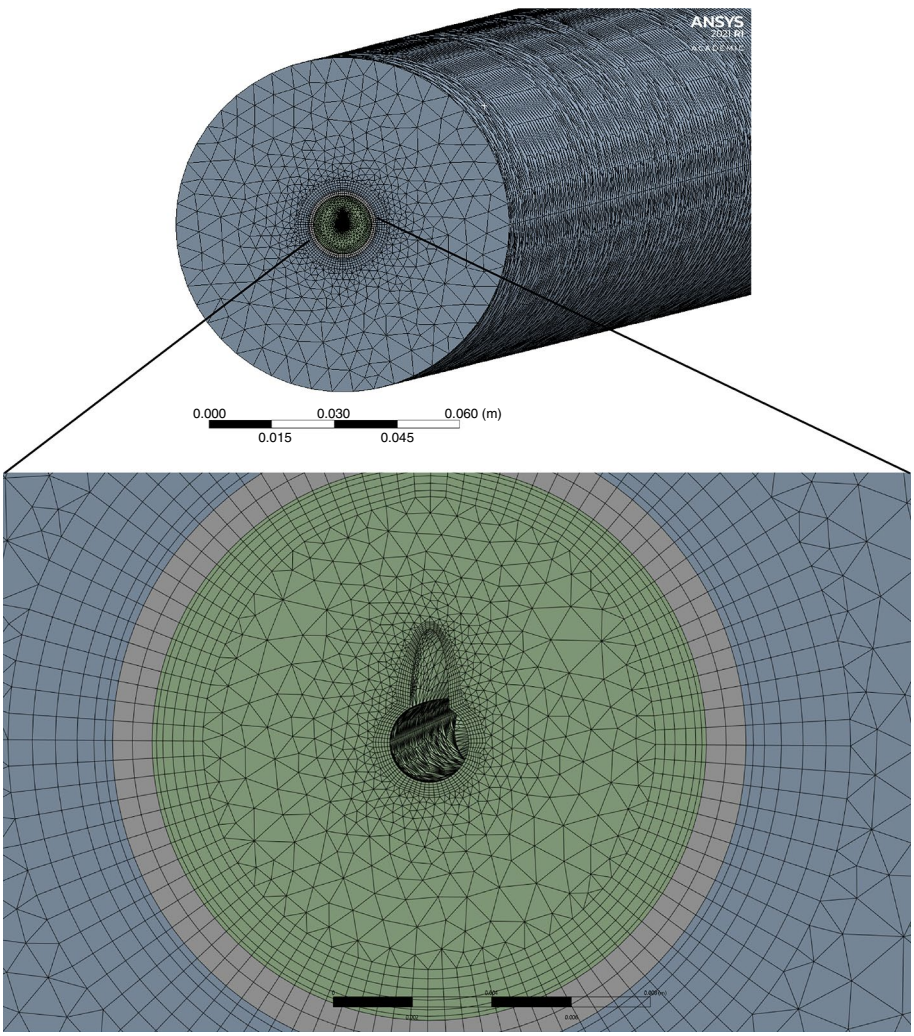

Fig. 4 Schematic of the overall domain featuring a grid with an oval helical turbulator

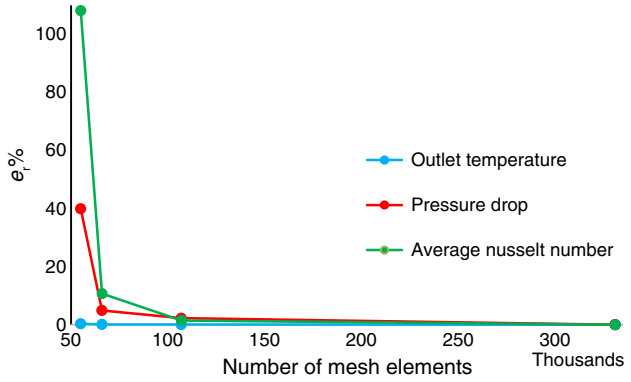

Fig. 5 Relative error of selected parameters for different mesh element counts in the transverse rectangular turbulator

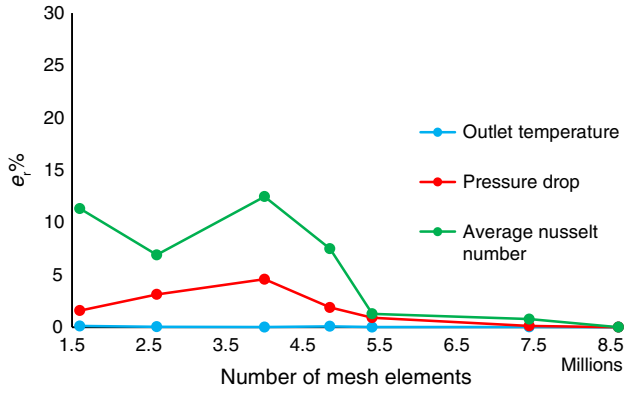

Fig. 6 Relative error of the selected parameters for different number of mesh elements for rectangular helical turbulator

Validation

To ensure the accuracy and reliability of the numerical framework, a comprehensive multi-level validation was performed, including empirical correlation, numerical, experimental nanofluid, and turbulator insertion validation. First, the predicted average Nusselt numbers and friction factors for laminar flow with pure water were compared against well-established empirical correlations proposed by Seider and Tate [64], Shah and London [67], Gnielinski [68], and Hausen [69]. Second, the nanofluid heat transfer results were numerically validated against the study of Bahmani et al. [70] with deviations remaining below 12% over a Reynolds number range of 100–2000. Third, experimental validation of nanofluid modeling was conducted by comparing the ratio of Nusselt numbers (nanofluid to pure water) with experimental data from Heyhat et al. [71] and two-phase numerical results from Shirvan et al. [72], where the single-phase model exhibited a maximum deviation of 5.42% relative to experiments. Finally, the accuracy of turbulator insertion modeling was assessed by comparison with the experimental twisted-tape data of Hong and Bergles [73], yielding discrepancies below 17.9%, which is within the acceptable range for laminar internal flows with inserts. Figure 7 presents the results of all validation stages.

Results and discussion

The investigation into the effects of transverse turbulator insertion has been previously conducted by Ebrahim [4]. This study presents the outcomes of helical turbulator insertion, with comparisons made to the results of transverse turbulator insertion where appropriate. This comparative analysis offers a clearer understanding of how different turbulator configurations affect the performance of the DTHE.

Figure 8 illustrates the average Nusselt number of the inner tube against Reynolds numbers for various helical turbulator shapes with SiO_2 nanofluid and a volume fraction 0.05 as the working fluid. In all cases, the twist ratio, height, and width of the turbulators were 1 to 0.04, and 0.002, and 0.001 m, respectively. The results indicate that the use of nanofluids significantly increases the Nusselt number compared to pure water. This increase is further enhanced by the insertion of turbulators. Specifically, the helical triangular turbulator shows considerably higher Nusselt numbers than other shapes. Conversely, the oval, rectangular, and trapezoidal helical turbulators exhibit similar average Nusselt numbers, with the trapezoidal shape demonstrating the lowest value. The rise in the Nusselt number can be attributed to two primary factors. First, the nanoparticles enhance the thermal properties of the fluid. Second, the turbulators induce additional mixing and secondary flows, reducing the thermal boundary layer near the wall. The distinct geometry of helical triangular turbulators generates more intense secondary flows and turbulence within the fluid. This effect arises because the sharp angles of the triangular turbulators disrupt the flow more effectively than smoother shapes, such as ovals, rectangles, or trapezoids. This disruption diminishes the thickness of the thermal boundary layer, thereby enhancing the rate of heat transfer. Moreover, the Nusselt number rises as the Reynolds number increases, attributed to the enhancement in momentum and fluid mixing. The combined influence of nanoparticles and turbulator insertion significantly improves the heat transfer performance of the DTHE.

Figure 9 depicts the pressure drop across the inner tube against Reynolds numbers for various helical turbulator shapes using SiO_2 nanofluid with a volume fraction of 0.05 as the working fluid. For all cases, the twist ratio, height, and width of the turbulators were 1, 0.04, 0.002, and 0.001 m, respectively. As it can be seen, the addition of nanoparticles to the working fluid results in an increased pressure drop compared to pure water, an effect that is accentuated

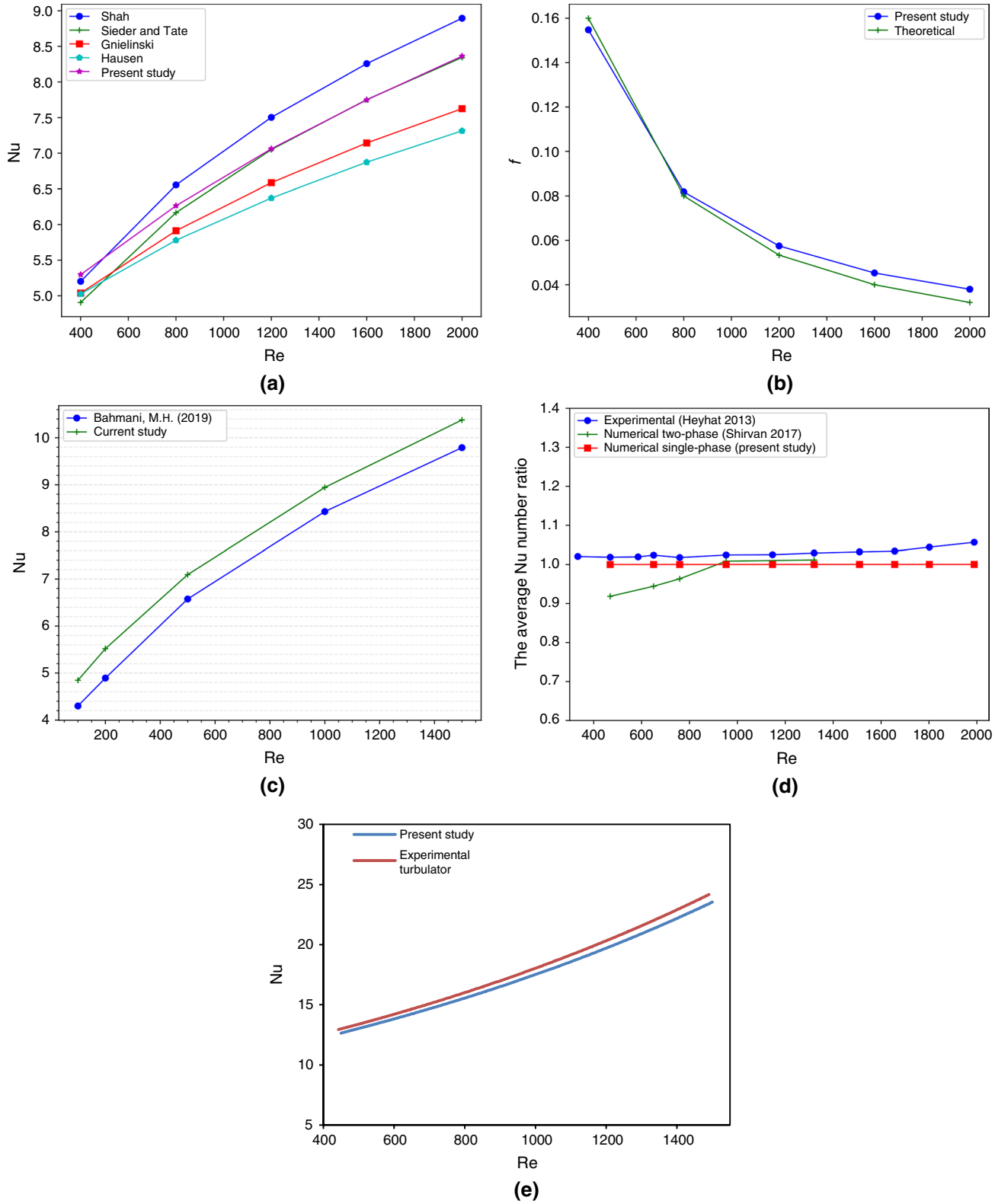

Fig. 7 Validation of the numerical model: **a** empirical correlation validation, **b** friction factor validation, **c** numerical validation of nanofluid, **d** experimental validation of nanofluid modeling, and **e** experimental validation of turbulator insertion

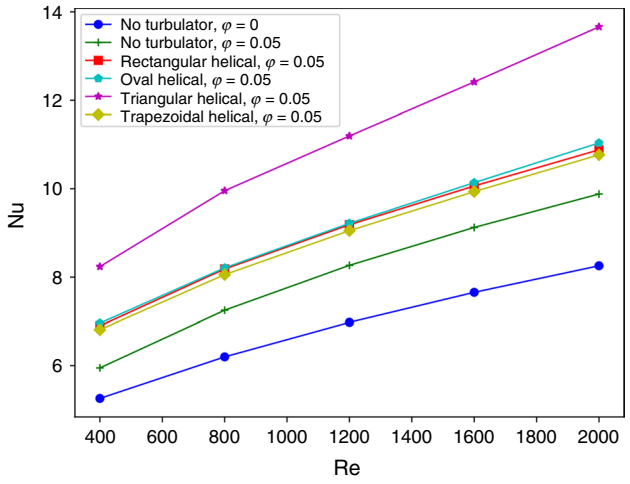

Fig. 8 The average Nusselt number against Reynolds numbers for various helical turbulators, SiO_2 nanofluid $\varphi = 0.05$, twisted ratio 1 to 0.04 m, $w = 0.001$ m, and $H = 0.29$

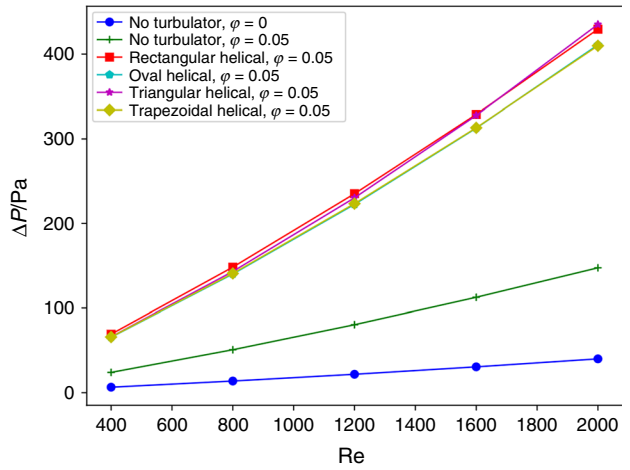

Fig. 9 The pressure drop against Reynolds numbers for various shapes of helical turbulators, SiO_2 nanofluid $\varphi = 0.05$, twisted ratio 1 to 0.04 m, $w = 0.001$ m, and $H = 0.29$

by the insertion of a helical turbulator into the DTHE. The figure reveals that the pressure drops for all helical turbulator shapes are approximately the same; however, the helical triangular and rectangular turbulators exhibit the highest pressure drop, while the helical oval and trapezoidal turbulators demonstrate the lowest values. This discrepancy can be attributed to the varying surface areas of each turbulator shape, indicating that the oval and trapezoidal turbulators create less friction compared to the rectangular and triangular turbulators.

Figure 10 displays color plots that show the velocity magnitude and temperature contour for various helical shapes, triangular, trapezoidal, rectangular, and oval, utilizing SiO_2 nanofluid at a Reynolds number of 1200 and a volume fraction $\varphi = 0.05$. The results indicate that changes in velocity magnitude are more significant in the triangular and oval helical shapes compared to the rectangular and trapezoidal shapes. Furthermore, the rectangular and trapezoidal shapes maintain a more uniform temperature distribution than the triangular and oval shapes. This discrepancy can be attributed to the more intense secondary and swirl flows observed in the triangular and oval shapes, which disrupt the thermal boundary layer after passing the helical ribs, leading to sharper temperature gradients, especially noted in the triangular configurations.

Figure 11 depicts the PEC of DTHE for various helical shapes, triangular, trapezoidal, rectangular, and oval, using SiO_2 nanofluid at a Reynolds number of 1200 and a volume fraction $\varphi = 0.05$. The results indicate that the triangular helical shapes exhibit the highest PEC, reaching up to 1.2, surpassing the other helical shapes. In contrast, the oval, trapezoidal, and rectangular shapes yield PEC values below unity, which are also lower than the case without turbulator insertion using nanofluid alone, indicating that under these conditions, the pressure penalty outweighs the heat transfer enhancement. The superior performance of the triangular geometry is attributed to its sharp edges, which promote stronger flow separation, more intense secondary vortices, and repeated disruption of the thermal boundary layer, leading to a higher heat transfer gain relative to friction losses. The oval geometry induces smoother but still effective swirling flow with reduced separation intensity, resulting in moderate PEC values, whereas the trapezoidal and rectangular shapes generate weaker vortex structures and larger stagnation regions, increasing friction without proportional heat transfer improvement. Consequently, the balance between boundary-layer disruption and pressure drop penalty governs the observed PEC ranking among the turbulator shapes.

Figure 12 illustrates the variation in the average Nusselt number within the inner tube for different ratios of the height of the triangular helical turbulator to the radius of the inner tube (H), using SiO_2 nanofluid at a Reynolds number of 1200 and a volume fraction $\varphi = 0.05$. It is observed that the Nusselt number increases with H. This increase can be attributed to enhanced secondary and swirl flows due to greater flow obstruction from the triangular helical shape, which reduces the thermal boundary-layer thickness and enhances heat transfer. A notable increase is observed at $H = 0.57$, where the average Nusselt number exceeds 44, indicating a substantial improvement at this specific H value compared to others.

Figure 13 presents the pressure drop in the inner tube for different ratios of the height of the triangular helical turbulator to the radius of the inner tube (H), using SiO_2 nanofluid at a Reynolds number of 1200 and a volume fraction $\varphi = 0.05$. The pressure drop escalates with increasing H, correlating with the increased obstruction caused by the taller

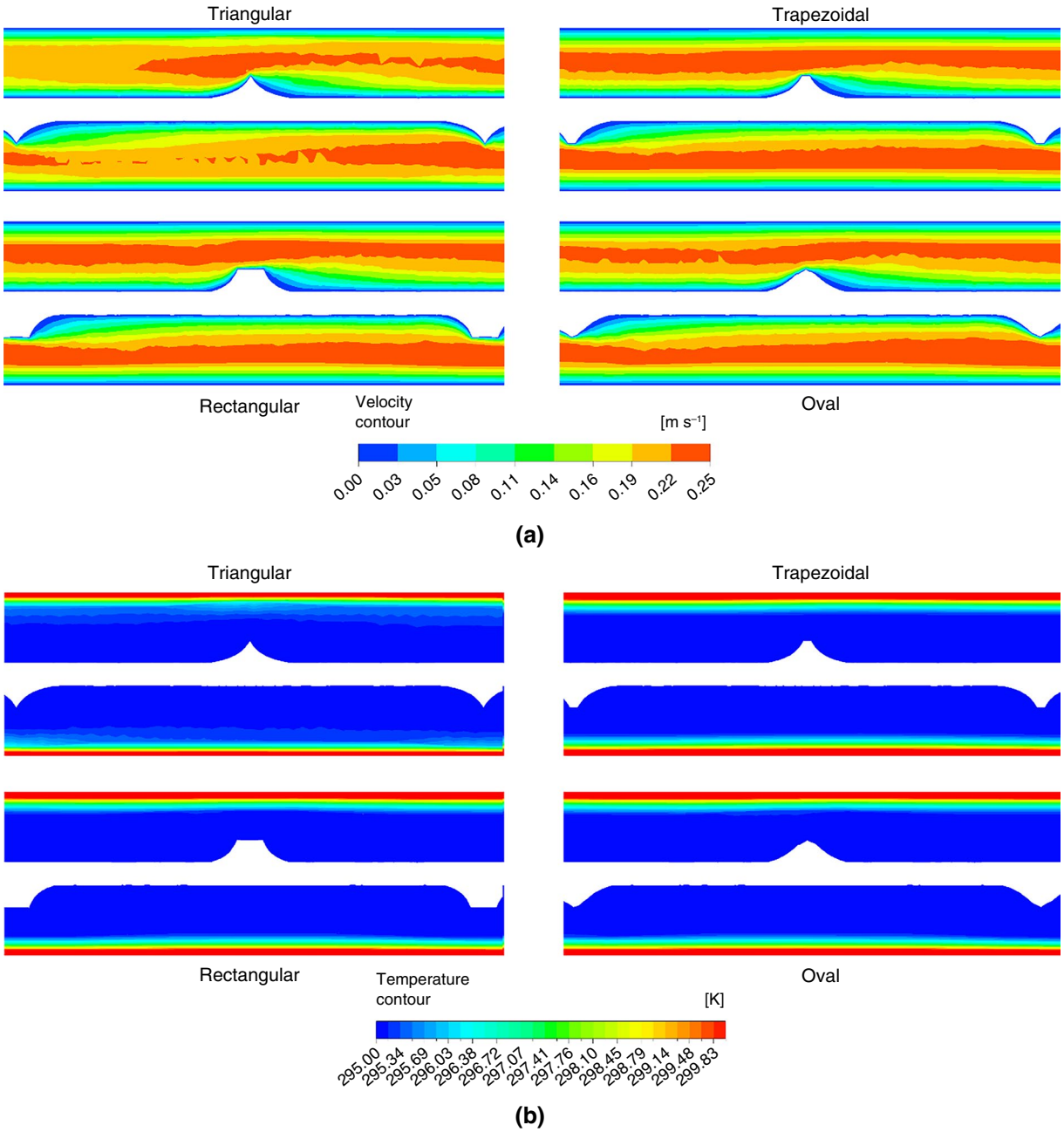

Fig. 10 Color plots of **a** velocity magnitude and **b** static temperature for different shapes of helical turbulators, utilizing SiO_2 nanofluid at Re = 1200, $\varphi = 0.05$, twisted ratio 1 to 0.04 m, $w = 0.001$ m, and $H = 0.29$

helical turbulators. The most significant impact is noted at $H = 0.71$, where the flow encounters maximum obstruction, leading to the highest pressure drop up to 648 Pa.

Figure 14 shows the maximum PEC for different ratios of the height of the triangular helical turbulator to the radius of the inner tube (H), using SiO_2 nanofluid at a Reynolds number of 1200 and a volume fraction $\varphi = 0.05$. It is evident that the PEC values exceed 1 in all scenarios, indicating that enhancement in heat transfer predominates over the increase in friction factor. Furthermore, an increase in the height of the helical turbulator results in higher PEC values, reaching up to 3.17 when $H = 0.71$. This suggests that the swirl flow significantly boosts the heat transfer rate with only a minimal rise in friction factor, thus optimizing the performance of the DTHE.

Figure 15 illustrates the bulk temperature within the inner tube for different ratios of the height of the triangular helical turbulator to the radius of the inner tube (H), using SiO_2 nanofluid at a Reynolds number of 1200 and a volume fraction $\varphi = 0.05$. The graph shows that as the height

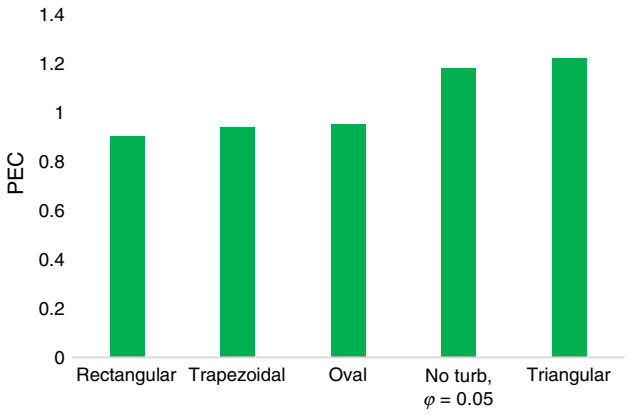

Fig. 11 PEC of different shapes of helical turbulators utilizing SiO_2 nanofluid at Re = 1200, $\varphi = 0.05$, twisted ratio 1 to 0.04 m, $w = 0.001$ m, and $H = 0.29$

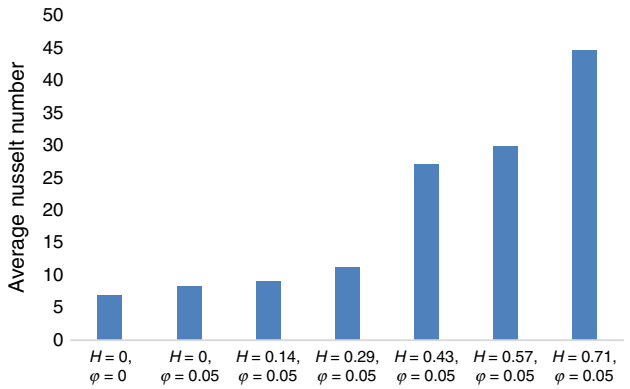

Fig. 12 Average Nusselt number of the inner tube for different ratios of the height of the triangular helical turbulator to the radius of the inner tube (H), using SiO_2 nanofluid at a Reynolds number of 1200 and a volume fraction $\varphi = 0.05$

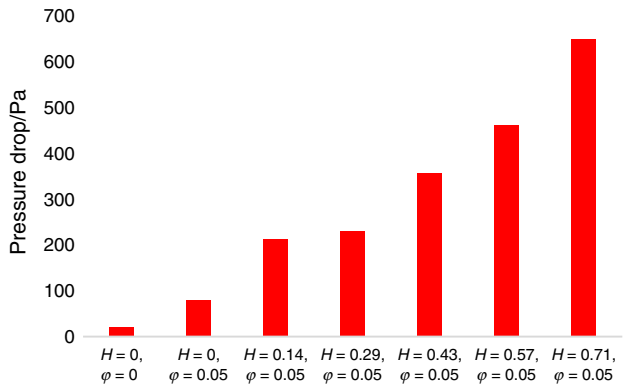

Fig. 13 Pressure drop of the inner tube for different ratios of the height of the triangular helical turbulator to the radius of the inner tube (H), using SiO_2 nanofluid at a Reynolds number of 1200 and a volume fraction $\varphi = 0.05$

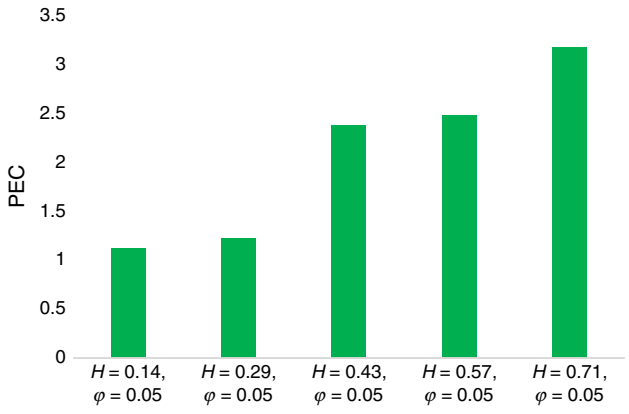

Fig. 14 Maximum PEC for different ratios of the height of the triangular helical turbulator to the radius of the inner tube (H), using SiO_2 nanofluid at a Reynolds number of 1200 and a volume fraction $\varphi = 0.05$

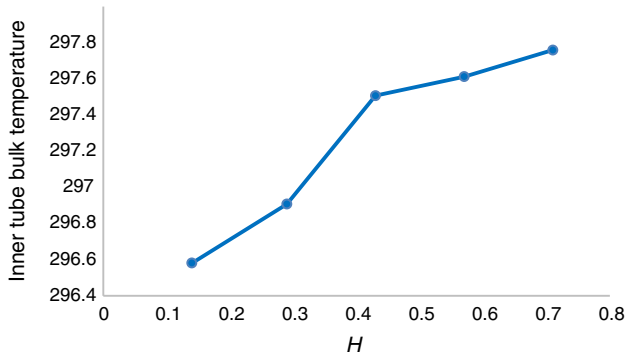

Fig. 15 Bulk temperature within the inner tube for different H, using SiO_2 nanofluid at a Reynolds number of 1200 and a volume fraction $\varphi = 0.05$

of the helical turbulators increases, the bulk temperature of the inner tube also increases. This is because higher helical turbulators enhance secondary and swirl flows within the inner fluid. These flows improve the distribution of heat transferred from the outer tube to the inner fluid. Consequently, the bulk temperature for $H = 0.71$ is closer to the temperature of the outer fluid, while for $H = 0.14$, there is a maximum difference between the outer fluid temperature and the inner fluid bulk temperature.

Figure 16 displays color plots representing a) the velocity in the x-direction, b) the velocity in the z-direction, and c) the static temperature at different heights of a triangular helical turbulator using a SiO_2 nanofluid with a volume fraction $\varphi = 0.05$. The data suggest that increasing the height of the helical turbulator leads to a more uniform temperature distribution across the flow. This uniformity is primarily due to enhanced secondary and swirling flow patterns, which are promoted by taller obstacles in the flow path. These obstacles disrupt the thermal boundary layer at

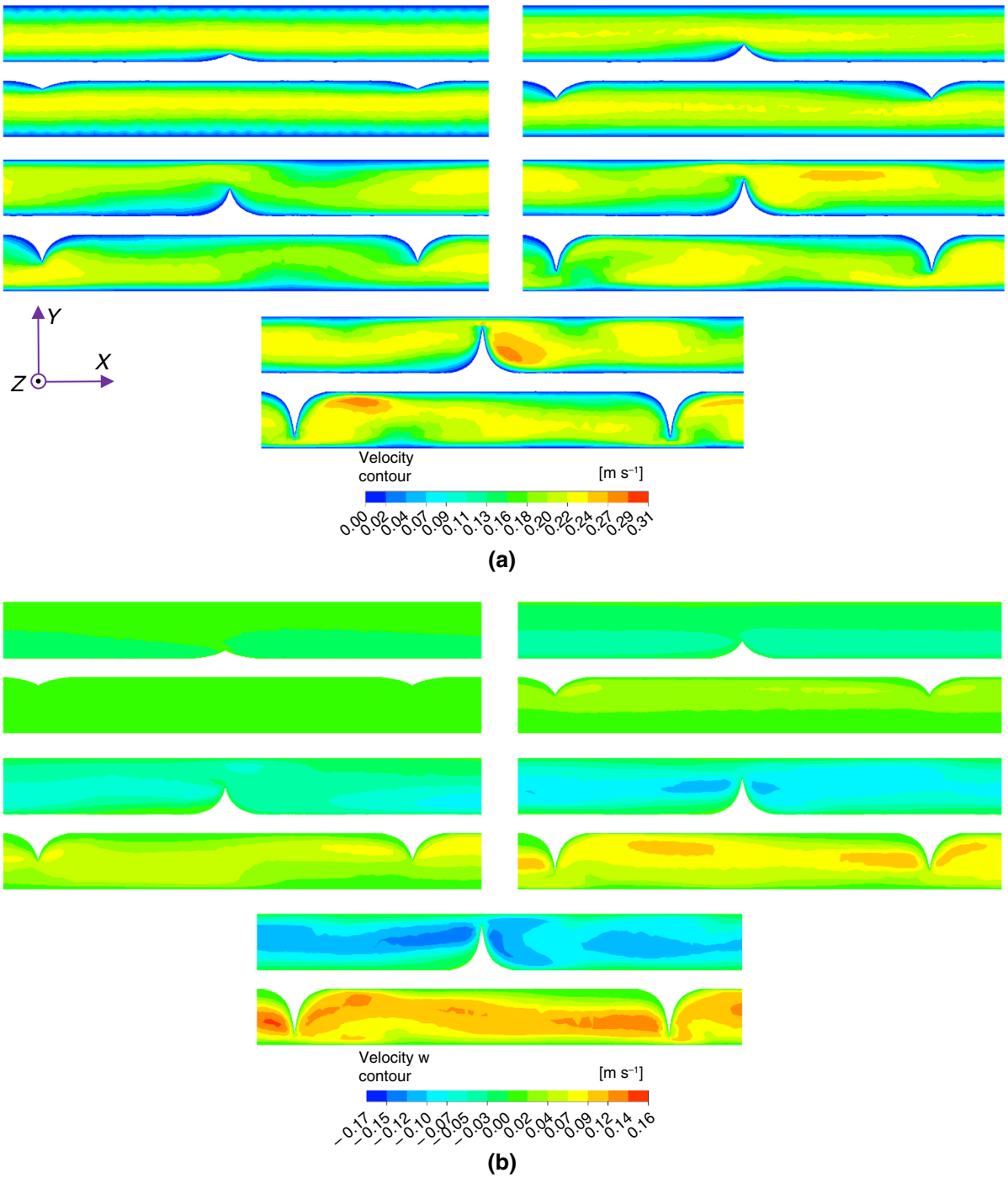

Fig. 16 Color plots of **a** the velocity in the x-direction, **b** the velocity in the z-direction, and **c** the static temperature at different heights of a triangular helical turbulator using a SiO_2 nanofluid at a Reynolds number of 1200 with a volume fraction $\varphi = 0.05$

each pitch, thinning it and thereby enhancing heat transfer rates within the system. However, increasing the height of the helical turbulator also intensifies the velocity in the z-direction, induces vortices, and slows the flow velocity, which results in a higher pressure drop across the system.

Comparison between transverse and helical turbulator

This section compares the effects of two types of turbulators, transverse and helical, on the performance of the DTHE.

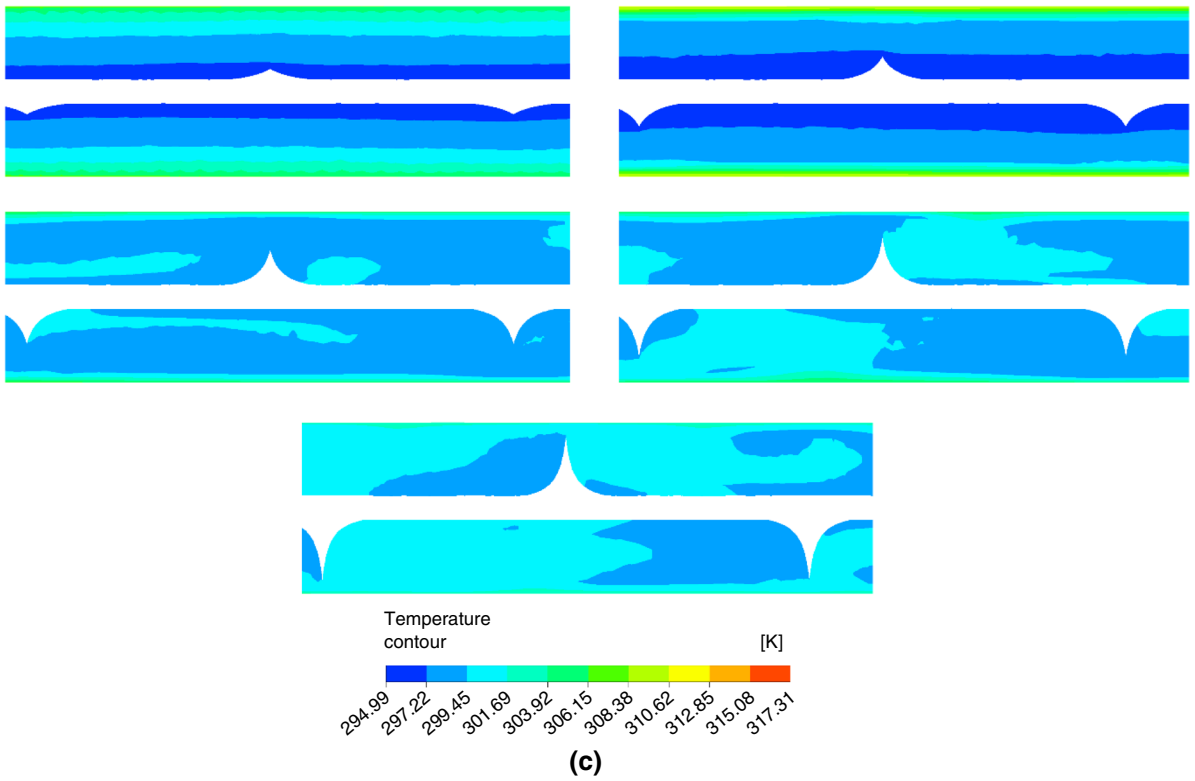

Fig. 16 (continued)

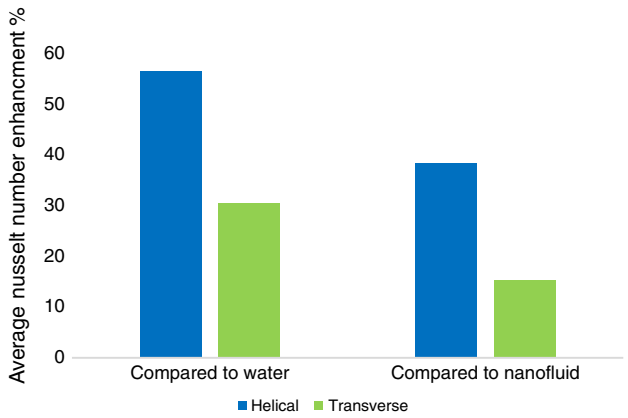

Fig. 17 Enhancement in the average Nusselt number when a combination of SiO_2 nanofluid ($\varphi = 0.05$) and both types of turbulators (in triangular shape) is used, relative to pure water and the same nanofluid without any turbulators at a Reynolds number of 400

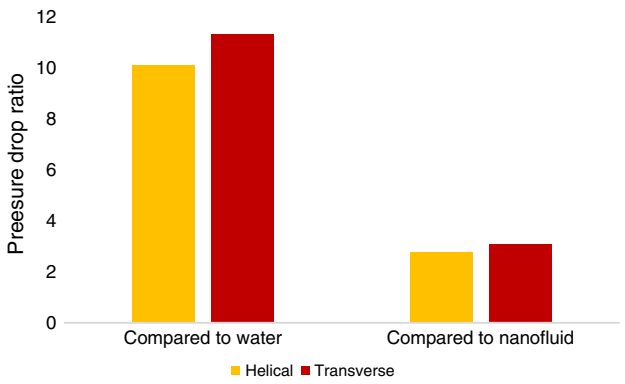

Fig. 18 Increase in the pressure drop when a combination of SiO_2 nanofluid ($\varphi = 0.05$) and both types of turbulators (in triangular shapes) is used, relative to pure water and the same nanofluid without any turbulators at a Reynolds number of 400

Figure 17 illustrates the enhancement in the average Nusselt number when a combination of SiO_2 nanofluid ($\varphi = 0.05$) and both types of turbulators (in triangular shapes) is used, relative to pure water and the same nanofluid without any turbulators. The results show that the helical turbulator offers a greater enhancement in the Nusselt number than the transverse turbulator, both against pure water and the nanofluid without turbulator insertion. This enhancement is attributed to the helical turbulators not only disrupting the flow direction along the tube but also inducing a swirling motion. This swirling motion increases mixing and secondary flow and extends the contact time between the fluid and the tube's inner wall, compared to the transverse turbulator. Thus, helical turbulators demonstrate a more effective heat transfer rate than transverse turbulators.

Furthermore, Fig. 18 presents the pressure drop ratios for the DTHE employing both turbulator types, compared to configurations using only pure water and the nanofluid without turbulators. The findings indicate that the helical turbulator results in a smaller increase in pressure drop than the transverse turbulator. This difference is likely due to the helical design creating fewer flow obstructions and the swirling motion reducing pressure drops, unlike the direct flow disruption caused by the transverse turbulator. Consequently, it is concluded that helical turbulators enhance the heat transfer rate more effectively by producing a lower pressure drop compared to transverse turbulators.

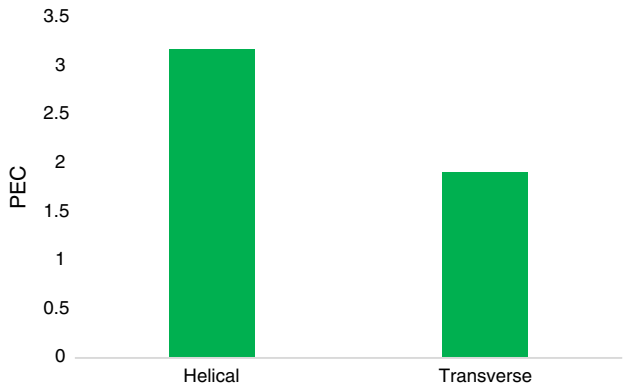

Fig. 19 Maximum PEC achieved with both transverse and helical turbulators

Figure 19 illustrates the maximum PEC achieved with both transverse and helical turbulators. As previously mentioned, the Nusselt number enhancement is greater for the helical turbulator, while the increase in pressure drop is more significant for the transverse turbulator. Thus, it can be inferred that the helical turbulator provides a better PEC. Specifically, the highest PEC value for the helical turbulator, at 3.17, is observed with a triangular shape using SiO_2 nanofluid and an H value of 0.71. Conversely, the maximum PEC of 1.9 for the transverse turbulator is achieved with a trapezoidal shape using the same height and nanofluid.

Figure 20 presents the streamlines in both transverse and helical turbulators for a rectangular shape case. It is apparent that the streamlines in the helical turbulator navigate around the turbulators more smoothly compared to the direct disruption caused by the transverse turbulators, which results in vortices forming behind the ribs. Additionally, it demonstrates that the flow path line in the helical turbulator is longer over the same distance compared to the transverse turbulator. This results in the fluid being in contact with the inner tube wall for a longer period, thereby enhancing heat exchange with the hot fluid in the outer tube.

Comparative analysis of results

In this section, the results and outcomes of the current research are compared with other published works, focusing on the most recent studies. As previously discussed,

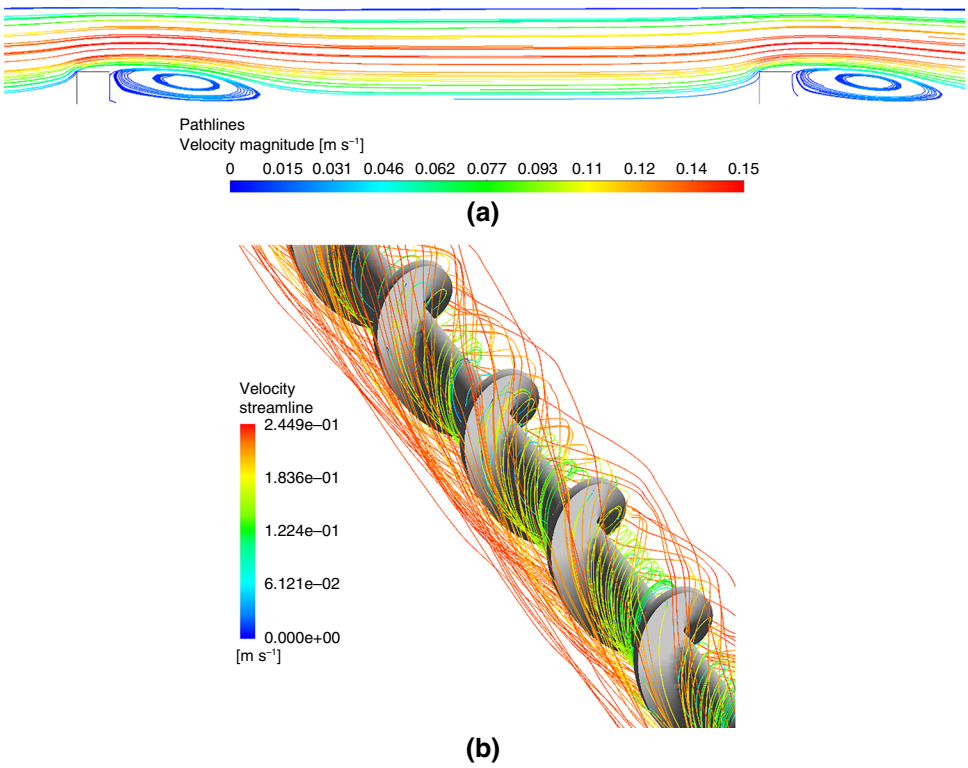

Fig. 20 Streamlines in both **a** transverse and **b** helical turbulators for a rectangular shape case

enhancing heat transfer in heat exchangers can be categorized into three main methods: passive, active, and combined. Generally, active methods yield a greater increase in heat transfer compared to passive methods due to the utilizing of external forces and power. Conversely, passive methods, which do not rely on external forces, offer advantages such as lower costs and easier maintenance. This section aims to quantify the increment in heat transfer for passive, active, and combined methods and compare these increments with the results obtained in this study. This comparative analysis provides a clearer understanding of how the findings of this research align with real-world applications and the extent to which they are practical and effective. By systematically comparing the heat transfer enhancement achieved through different methods, this analysis underscores the practical relevance and applicability of the study's results. The findings from this research are evaluated against the backdrop of existing literature to highlight their significance and potential impact on the field of heat transfer enhancement in heat exchangers. This approach ensures a comprehensive assessment of the study's contributions and situates its results within the broader context of ongoing research and technological advancements.

- Passive method

The passive method of enhancing heat transfer can be categorized into four main techniques: using nanofluids, turbulator insertion, geometry modifications, and extended surface areas (fins). In this study, we employed turbulator insertion and nanofluids to investigate the enhancement of the heat transfer rate in a DTHE. Recent studies from each technique were reviewed to compare the percentage increase in heat transfer with the enhancements observed in this study.

Yogaraj et al. [74] used zinc oxide and titanium oxide nanofluids with ethylene glycol as the base fluid in a counterflow DTHE, achieving a maximum heat transfer enhancement of 18.5% for zinc oxide. Marzouk et al. [75] designed a turbulator using a one-meter steel nail rod in a DTHE, focusing on the pitch length of the nail rods, and achieved a maximum heat transfer enhancement of 90%. Chaurasiya et al. [76] used corrugated tubes for the inner and outer tubes of a DTHE, implementing different helix angles, and achieved a maximum PEC of 1.17 and a 33% improvement in the Nusselt number. Firoozeh et al. [77] employed the geometry change technique on the inner tube of a DTHE by varying the groove angles to improve the heat transfer rate. This investigation explored different groove angles and achieved a maximum enhancement of 32% in the heat transfer rate. Ashraf et al. [78] utilized the extended surface area technique with arrow fins to enhance the performance of a DTHE. The study investigated varying numbers and heights of arrow fins and achieved a maximum improvement of 113.2% in the heat transfer rate. Sharaf et al. [79] used a combination of techniques, including turbulator insertion, geometry change, and nanofluid, to enhance the heat transfer rate of a helical DTHE. A spring wire was inserted, and silicon dioxide nanofluid with water as the base fluid was used, resulting in a maximum heat transfer rate increase of 174%.

- Active method

Jawarneh et al. [80] conducted an experimental study using the active method to enhance heat transfer in a DTHE by utilizing jet vortex flow. By employing a vortex generator to create swirl flow with inclined holes and different inlet angles, a maximum heat transfer enhancement of 82% was achieved. Li et al. [81] applied an audible acoustic field to enhance heat transfer in a DTHE. Investigating various parameters including sound pressure level and acoustic frequency, a maximum efficiency of 76.22% was achieved.

- Combined method

Maleki et al. [11] combined passive and active methods to enhance heat transfer in a DTHE. Using a wire oscillator inside the inner tube as an electromagnetic vibration source and copper oxide nanofluid, a maximum heat transfer enhancement of 277.5% and a maximum PEC of 3.92 were achieved. Hedeshi et al. [82] used ultrasonic vibration combined with a nanofluid in a DTHE. Employing ultrasonic waves at a frequency of 40 kHz and a power of 60 watts, along with aluminum oxide nanofluid, the thermal system efficiency of the DTHE was improved by up to 42.3%. Table 3 provides a summary of recent studies employing various methods, including passive, active, and combined approaches, to enhance the heat transfer rate in DTHEs.

From the table, it is evident that different methods offer varying levels of heat transfer enhancement in DTHEs. This study focused on a combination of turbulator insertion and nanofluids as passive method to enhance heat transfer rates. Specifically, the increase in heat transfer due to the use of nanofluids alone in this study was 18.43%. When combined with helical turbulator insertion, the heat transfer enhancement reached up to 560% compared to using pure water without any turbulator insertion. Additionally, the maximum PEC achieved in this study was 3.17.

Comparing these results with those in Table 3 shows that the technique employed in this study provides a substantial enhancement. However, the PEC for the combined methods in other studies is higher, likely due to the advantages of using external forces and power. Furthermore, comparing the results of this study with those from the literature review for passive methods (as shown in Fig. 21) indicates that the enhancement achieved in this study surpasses the average

Table 3 Recent studies on heat transfer enhancement methods

Author	Method	Heat transfer enhancement /% or PEC
Yogaraj et al. [74]	Passive: Nanofluid	18.5
Sharaf et al. [83]	Passive: Turbulator insertion	112
Dhumal and Havaldar [84]	Passive: Turbulator insertion	315 PEC: 3.06
Marzouk et al. [75]	Passive: Turbulator insertion	90
Chaurasia and Sarviya [85]	Passive: Turbulator insertion	100 PEC: 1.5
Dandoutiya and Kumar [86]	Passive: Turbulator insertion	105.47 PEC: 1.35
Ali and Shehab [87]	Passive: Geometry change	50 PEC: 9.07
Zhang et al. [88]	Passive: Geometry change	PEC: 3.2
Firoozeh et al. [77]	Passive: Geometry change	32
Chaurasiya et al. [76]	Passive: Geometry change	33 PEC: 1.17
Hasan et al. [89]	Passive: Extended surface area (fin)	210
Ashraf et al. [78]	Passive: Extended surface area (fin)	113.2
Sharaf et al. [79]	Passive: Combined techniques	174
Izadi et al. [90]	Passive: Combined techniques	11.91
Jawarneh et al. [80]	Active	82
Li et al. [81]	Active	76.22
Maleki et al. [11]	Combined	277.5 PEC: 3.92
Hedeshi et al. [82]	Combined	42.3 PEC: 1.42
Azizi et al. [91]	Combined	15

increase in heat transfer from various passive techniques. This demonstrates the effectiveness of the current turbulator designs and justifies their use. In conclusion, the combination of turbulator insertion and nanofluids used in this study significantly improves heat transfer rates in DTHEs, providing a competitive alternative to other enhancement methods. The results underscore the potential of these techniques to enhance thermal performance in practical applications.

Conclusions

This study presented a comprehensive numerical investigation of heat transfer and fluid flow characteristics in a double tube heat exchanger using SiO_2 nanofluids and various turbulator designs, conducted via CFD simulations in ANSYS Fluent (2023). A single-phase model and a coupled velocity–pressure solver with second-order upwind schemes were applied to analyze the performance impacts of both transverse and helical turbulator configurations. The findings clearly demonstrate the comparative benefits of using nanofluids and turbulator inserts:

- Nanofluid performance without turbulators: SiO_2 nanofluid alone enhanced the heat transfer rate by 18.4%, achieving a performance evaluation criterion (PEC) of 1.18, indicating a moderate yet effective improvement compared to base fluid conditions.
- Helical turbulators, especially the triangular helical design, significantly improved heat transfer performance, increasing the Nusselt number by approximately 565%, while maintaining lower pressure drops due to efficient swirl generation.
- Transverse turbulators (trapezoidal shapes) also showed strong enhancement, with up to 470% increase in the Nusselt number, though generally accompanied by higher pressure losses.
- Turbulator height was found to be a critical parameter affecting both the Nusselt number and friction factor. Higher turbulator heights typically increased thermal performance but also introduced greater flow resistance.
- Helical turbulator configurations achieved a maximum PEC of 3.17, compared to 1.9 for the best transverse design, confirming that helical inserts offer superior thermal–hydraulic performance.

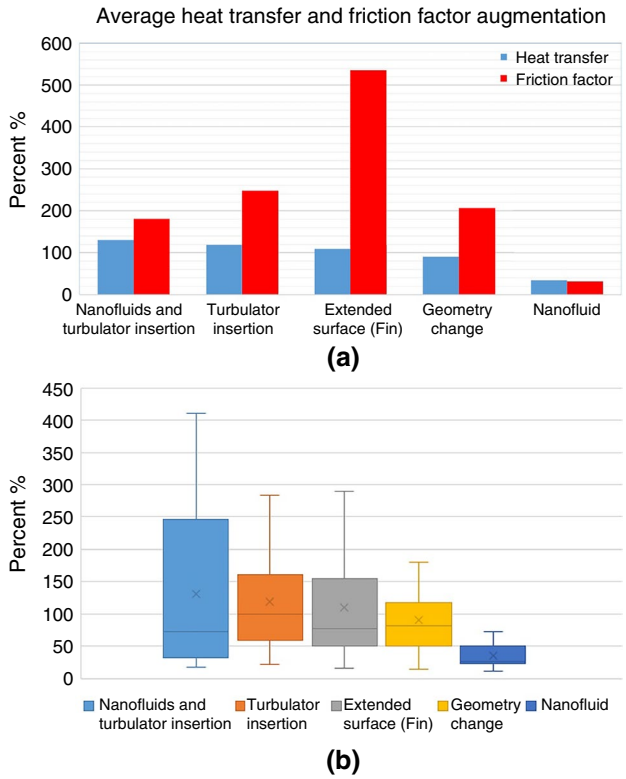

Fig. 21 Statistical investigation presented by Tavousi et al. [18] **a** increase in heat transfer and friction factor and **b** increase in heat transfer of different techniques (box-and-whisker plot)

These results offer valuable design insights for optimizing double tube heat exchangers, particularly in industrial and engineering applications involving laminar or low-Reynolds-number operation. The use of nanofluids combined with optimally shaped helical turbulators can significantly enhance heat transfer performance while maintaining manageable pressure drops, supporting more efficient and compact heat exchanger designs. Future work will involve experimental validation using a scaled double tube heat exchanger with interchangeable helical inserts to further assess practical feasibility and measurement uncertainties.

Acknowledgements The authors thank Dr Roger Tait for his advice and guidance on the use of the High Performance Computing (Cluster 3) resource. The authors also thank the School of Architecture, Built Environment, Computing and Engineering at Birmingham City University for supporting this High Performance Computing resource.

Author contribution E.T. Methodology, Software, Validation, and Writing – original draft. N.P. Supervision, Methodology, Resources, and Writing – review & editing. M.R. Supervision, Formal analysis, and review & editing. R.H. Supervision, Project administration, and review & editing. D.F. Supervision and review & editing.

Funding This research received no external funding.

Data availability No datasets were generated or analysed during the current study.

Declarations

Conflict of interest The authors declare no competing interests.

References

1. Sarafraz M, Christo F, Tran N, Fulcheri L, Hessel V. Conversion of greenhouse gases to synthetic fuel using a sustainable cyclic plasma process. Int J Hydrogen Energy. 2023;48(16):6174–91.
2. Li H, et al. A comprehensive review of heat transfer enhancement and flow characteristics in the concentric pipe heat exchanger. Powder Technol. 2022;397:117037.
3. Hosseinzadeh K, Moghaddam ME, Asadi A, Mogharrebi A, Ganji D. Effect of internal fins along with hybrid nano-particles on solid process in star shape triplex latent heat thermal energy storage system by numerical simulation. Renew Energy. 2020;154:497–507.
4. Esmaeili Z, Vahidhosseini SM, Rashidi S. A novel design of double pipe heat exchanger with innovative turbulator inside the shell-side space. Int Commun Heat Mass Transf. 2024;155:107523.
5. Moradkhani M, Hosseini SH, Mansouri M, Ahmadi G, Song M. Robust and universal predictive models for frictional pressure drop during two-phase flow in smooth helically coiled tube heat exchangers. Sci Rep. 2021;11(1):20068.
6. Louis SP, Ushak S, Milian Y, Nemś M, Nemś A. Application of nanofluids in improving the performance of double-pipe heat exchangers—a critical review. Materials. 2022;15(19):6879.
7. Soheibi H, Shomali Z, Ghazanfarian J. Combined active-passive heat transfer control using slotted fins and oscillation: the cases of single cylinder and tube bank. Int J Heat Mass Transf. 2022;182:121972.
8. Maleki NM, Pourahmad S, Tavousi E, Perera N, Talebizadehsardari P, Keshmiri A. Thermal-frictional behavior of solid magnetic strip turbulator and helical coiled wire turbulator inside a double tube heat exchanger. Int Commun Heat Mass Transf. 2025;161:108406.
9. Maleki NM, Pourahmad S. Heat transfer enhancement in a heated copper tube using the electromagnetic vibration method for nanofluids as working fluid: an experimental study. Int Commun Heat Mass Transf. 2023;141:106566.
10. Setareh M, Saffar-Avval M, Abdullah A. Experimental and numerical study on heat transfer enhancement using ultrasonic vibration in a double-pipe heat exchanger. Appl Therm Eng. 2019;159:113867.
11. Maleki NM, Pourahmad S, Khoshkhoo RH, Ameri M. Performance improvement of a double tube heat exchanger using novel electromagnetic vibration (EMV) method in the presence of

Al2O3-water and CuO-water nanofluid; an experimental study. Energy. 2023;281:128193.
12. Bezaatpour M, Goharkhah M. Convective heat transfer enhancement in a double pipe mini heat exchanger by magnetic field induced swirling flow. Appl Therm Eng. 2020;167:114801.
13. Lalegani F, Saffarian MR, Moradi A, Tavousi E. Effects of different roughness elements on friction and pressure drop of laminar flow in microchannels. Int J Numer Methods Heat Fluid Flow. 2018;28(7):1664–83. https://doi.org/10.1108/HFF-04-2017-0140.
14. Gnanavel C, Saravanan R, Chandrasekaran M. Heat transfer enhancement through nano-fluids and twisted tape insert with rectangular cut on its rib in a double pipe heat exchanger. Mater Today Proc. 2020;21:865–9.
15. Banihashemi S, Assari M, Javadi S, Vahidifar S. Study the effect of innovative active and passive methods on thermal characteristics and turbulent flow behaviour in a heat exchanger pipe. J Therm Anal Calorim. 2024;149(2):777–97.
16. Alam T, Kim M-H. A comprehensive review on single phase heat transfer enhancement techniques in heat exchanger applications. Renew Sustain Energy Rev. 2018;81:813–39.
17. Al-darraji AR, Marzouk S, Aljabr A, Almehmadi FA, Alqaed S, Kaood A. Enhancement of heat transfer in a vertical shell and tube heat exchanger using air injection and new baffles: experimental and numerical approach. Appl Therm Eng. 2024;236:121493.
18. Tavousi E, Perera N, Flynn D, Hasan R. Heat transfer and fluid flow characteristics of the passive method in double tube heat exchangers: a critical review. Int J Thermofluids. 2023. https://doi.org/10.1016/j.ijft.2023.100282.
19. Pourahmad S, Pesteei S. Effectiveness-NTU analyses in a double tube heat exchanger equipped with wavy strip considering various angles. Energy Convers Manag. 2016;123:462–9.
20. Tavousi E, Perera N, Flynn D, Hasan R, Rahman M. Effect of novel turbulators on the hydrothermal performance of counterflow double tube heat exchanger using nanofluids. Int J Heat Fluid Flow. 2024;107:109427.
21. Pourahmad S, Pesteei S, Ravaeei H, Khorasani S. Experimental study of heat transfer and pressure drop analysis of the air/water two-phase flow in a double tube heat exchanger equipped with dual twisted tape turbulator: simultaneous usage of active and passive methods. J Energy Storage. 2021;44:103408.
22. Song K, He Y, Zhang Q, Wu X, He A, Hou Q. Thermal performance promotion of a novel double-tube heat exchanger by helical fin with perforations. Int Commun Heat Mass Transf. 2024;150:107189.
23. Tian Z, Song K, Sun K, Hou Q, Luo C, Tagawa T. Numerical investigation of thermal characteristics of double-tube heat exchangers with alternate twist direction and different phase angles of the inner oval tube. Appl Thermal Eng. 2024;255:123979.
24. Tavousi E, Perera N, Flynn D, Hasan R. Numerical investigation of laminar heat transfer and fluid flow characteristics of Al2O3 nanofluid in a double tube heat exchanger. Int J Numer Methods Heat Fluid Flow. 2023. https://doi.org/10.1108/HFF-03-2023-0114.
25. E. Tavousi, N. Perera, D. Flynn, and R. Hasan, Numerical investigation of heat transfer and fluid flow characteristics of Al2O3 nanofluid In A double tube heat exchanger with turbulator insertion, Proceedings of the 9th world congress on mechanical, chemical, and material engineering (MCM'23), August 06 08 2023, https://doi.org/10.11159/htff23.218.
26. Kadhim SA, Ibrahim OAA-M, Al-Ghezi MK, Ashour AM. Critical review of the use of TiO_2 nanofluid as a heat transfer fluid in the double-pipe heat exchanger: SA Kadhim et al. J Therm Anal Calorim. 2025;150(16):11995–2015.
27. Singh SK, Sarkar J. Thermohydraulic behavior of concentric tube heat exchanger inserted with conical wire coil using mono/hybrid nanofluids. Int Commun Heat Mass Transfer. 2021;122:105134.
28. Choi SU, Eastman JA. Enhancing thermal conductivity of fluids with nanoparticles. Argonne, IL: Argonne National Lab(ANL); 1995.
29. Yu W, France DM, Routbort JL, Choi SU. Review and comparison of nanofluid thermal conductivity and heat transfer enhancements. Heat Transf Eng. 2008;29(5):432–60.
30. Atofarati EO, Sharifpur M, Huan Z, Awe OO, Meyer JP. Experimental and machine learning study on the influence of nanoparticle size and pulsating flow on heat transfer performance in nanofluid-jet impingement cooling. Appl Therm Eng. 2025;258:124631.
31. Adogbeji VO, Sharifpur M, Meyer JP. Experimental investigation into heat transfer and flow characteristics of magnetic hybrid nanofluid (Fe3O4/TiO2) in turbulent region. Appl Therm Eng. 2025;258:124630.
32. Atofarati EO, Sharifpur M, Meyer JP. Pulsating nanofluid-jet impingement cooling and its hydrodynamic effects on heat transfer. Int J Therm Sci. 2024;198:108874.
33. Alqaed S, Mustafa J, Sajadi SM, Almehmadi FA, Sharifpur M. The effect of turbulator holes diameter on heat transfer optimization of a geothermal heat exchanger by using nanofluid. Geothermics. 2024;119:102967.
34. Eiamsa-Ard S, Thianpong C, Eiamsa-Ard P, Promvonge P. Convective heat transfer in a circular tube with short-length twisted tape insert. Int Commun Heat Mass Transfer. 2009;36(4):365–71.
35. Saedodin S, Zaboli M, Rostamian SH, Kharabati S. Statistical analysis and shape optimization of a finned corrugated heat exchanger using RSM. Chem Eng Commun. 2023;210(5):716–39.
36. Gunes S, Ozceyhan V, Buyukalaca O. Heat transfer enhancement in a tube with equilateral triangle cross sectioned coiled wire inserts. Exp Therm Fluid Sci. 2010;34(6):684–91.
37. Noorbakhsh M, Zaboli M, Mousavi Ajarostaghi SS. Numerical evaluation of the effect of using twisted tapes as turbulator with various geometries in both sides of a double-pipe heat exchanger. J Therm Anal Calorim. 2020;140:1341–53.
38. Ibrahim E. Augmentation of laminar flow and heat transfer in flat tubes by means of helical screw-tape inserts. Energy Convers Manag. 2011;52(1):250–7.
39. Nakhchi M, Esfahani JA. Numerical investigation of different geometrical parameters of perforated conical rings on flow structure and heat transfer in heat exchangers. Appl Therm Eng. 2019;156:494–505.
40. Sheikholeslami M, Ganji D. Heat transfer improvement in a double pipe heat exchanger by means of perforated turbulators. Energy Convers Manag. 2016;127:112–23.
41. Kumar NR, Bhramara P, Sundar LS, Singh MK, Sousa AC. Heat transfer, friction factor and effectiveness of Fe3O4 nanofluid flow in an inner tube of double pipe U-bend heat exchanger with and without longitudinal strip inserts. Exp Therm Fluid Sci. 2017;85:331–43.
42. Hangi M, Rahbari A, Lipiński W. Design improvement of compact double-pipe heat exchangers equipped with tube-side helical insert and annulus-side helical strip: hydrothermal and exergy analyses. Appl Therm Eng. 2021;190:116805.
43. Hussein H, Freegah B, Saleh Q. Investigate the impact of different fin configurations arranged in-line on the double-pipe heat exchanger's hydrothermal response. Int J Heat Fluid Flow. 2025;115:109834.
44. Azizi AS, Jahanian O, Ajarostaghi SSM, Arıcı M. Employing uniform and non-uniform inner twisted elliptical tubes in a double-pipe heat exchanger. Int J Heat Fluid Flow. 2024;107:109384.
45. Eiamsa-ard S, Pethkool S, Thianpong C, Promvonge P. Turbulent flow heat transfer and pressure loss in a double pipe heat exchanger with louvered strip inserts. Int Commun Heat Mass Transf. 2008;35(2):120–9.

46. Lakew AA, Bolland O. Working fluids for low-temperature heat source. Appl Therm Eng. 2010;30(10):1262–8.
47. Padmanabhan S, Reddy OY, Yadav KVAK, Raja VB, Palanikumar K. Heat transfer analysis of double tube heat exchanger with helical inserts. Mater Today Proc. 2021;46:3588–95.
48. Eshgarf H, Nadooshan AA, Raisi A. A review of multi-phase and single-phase models in the numerical simulation of nanofluid flow in heat exchangers. Eng Anal Bound Elem. 2023;146:910–27.
49. Albojamal A, Vafai K. Analysis of single phase, discrete and mixture models, in predicting nanofluid transport. Int J Heat Mass Transf. 2017;114:225–37.
50. Razzaq I, et al. Nanofluids for advanced applications: a comprehensive review on preparation methods, properties, and environmental impact. ACS Omega. 2025;10(6):5251–82.
51. Ramesh G, Prabhu NK. Review of thermo-physical properties, wetting and heat transfer characteristics of nanofluids and their applicability in industrial quench heat treatment. Nanoscale Res Lett. 2011;6:1–15.
52. Zou T, et al. Preparation and performance of form-stable TBAB hydrate/SiO2 composite PCM for cold energy storage. Int J Refrig. 2019;101:117–24.
53. Incropera FP, DeWitt DP, Bergman TL, Lavine AS. Fundamentals of heat and mass transfer. New York: Wiley; 1996.
54. Mohammed H, Hasan HA, Wahid M. Heat transfer enhancement of nanofluids in a double pipe heat exchanger with louvered strip inserts. Int Commun Heat Mass Transf. 2013;40:36–46.
55. Tian L-L, Liu X, Chen S, Shen Z-G. Effect of fin material on PCM melting in a rectangular enclosure. Appl Therm Eng. 2020;167:114764.
56. Iwaniszyn M, et al. Entrance effects on forced convective heat transfer in laminar flow through short hexagonal channels: Experimental and CFD study. Chem Eng J. 2021;405:126635.
57. Akbari OA, Toghraie D, Karimipour A, Marzban A, Ahmadi GR. The effect of velocity and dimension of solid nanoparticles on heat transfer in non-Newtonian nanofluid. Phys E Low-Dimens Syst Nanostruct. 2017;86:68–75.
58. Kamyar A, Saidur R, Hasanuzzaman M. Application of computational fluid dynamics (CFD) for nanofluids. Int J Heat Mass Transfer. 2012;55(15–16):4104–15.
59. Bergman T. Effect of reduced specific heats of nanofluids on single phase, laminar internal forced convection. Int J Heat Mass Transfer. 2009;52(5–6):1240–4.
60. Vajjha RS, Das DK. Experimental determination of thermal conductivity of three nanofluids and development of new correlations. Int J Heat Mass Transfer. 2009;52(21–22):4675–82.
61. Sharma K, Sarma P, Azmi W, Mamat R, Kadirgama K. Correlations to predict friction and forced convection heat transfer coefficients of water based nanofluids for turbulent flow in a tube. Int J Microscale Nanoscale Therm Fluid Trans Pheno. 2012;3(4):1–25.
62. Lin J, Hong Y, Lu J. New method for the determination of convective heat transfer coefficient in fully-developed laminar pipe flow. Acta Mech Sin. 2022;38(1):1–10.
63. Ahmed HE, Ahmed M, Seder IM, Salman B. Experimental investigation for sequential triangular double-layered microchannel heat sink with nanofluids. Int Commun Heat Mass Transfer. 2016;77:104–15.
64. Sieder EN, Tate GE. Heat transfer and pressure drop of liquids in tubes. Ind Eng Chem. 1936;28(12):1429–35.
65. White FM. Fluid mechanics. Noida: Tata McGraw-Hill Education; 1979.
66. Noorbakhsh M, Ajarostaghi SSM, Zaboli M, Kiani B. Thermal analysis of nanofluids flow in a double pipe heat exchanger with twisted tapes insert in both sides. J Therm Anal Calorim. 2022;147(5):3965–76.
67. Shah RK, London AL. Laminar flow forced convection in ducts: a source book for compact heat exchanger analytical data. Cambridge: Academic press; 2014.
68. Gnielinski V. New equations for heat and mass transfer in turbulent pipe and channel flow. Int Chem Eng. 1976;16(2):359–67.
69. Hausen H. Neue Gleichungen fur die Warmeubertragung bei freier oder erzwungener Stromung. Allg Waermetech. 1959;9:75–9.
70. Bahmani MH, Akbari OA, Zarringhalam M, Shabani GAS, Goodarzi M. Forced convection in a double tube heat exchanger using nanofluids with constant and variable thermophysical properties. Int J Numer Methods Heat Fluid Flow. 2019. https://doi.org/10.1108/HFF-01-2019-0017.
71. Heyhat M, Kowsary F, Rashidi A, Momenpour M, Amrollahi A. Experimental investigation of laminar convective heat transfer and pressure drop of water-based Al2O3 nanofluids in fully developed flow regime. Exp Therm Fluid Sci. 2013;44:483–9.
72. Shirvan KM, Mamourian M, Mirzakhanlari S, Ellahi R. Numerical investigation of heat exchanger effectiveness in a double pipe heat exchanger filled with nanofluid: a sensitivity analysis by response surface methodology. Powder Technol. 2017;313:99–111.
73. Hong S, Bergles A. Augmentation of laminar flow heat transfer in tubes by means of twisted-tape inserts. J Heat Transf. 1976;98(2):251–6.
74. D. Yogaraj et al., Thermal performance analysis of a counter-flow double-pipe heat exchanger using titanium oxide and zinc oxide nanofluids, Materials Today: Proceedings, 2023.
75. Marzouk S, Almehmadi FA, Aljabr A, Sharaf MA. Numerical and experimental investigation of heat transfer enhancement in double tube heat exchanger using nail rod inserts. Sci Rep. 2024;14(1):9637.
76. Chaurasiya PK, et al. Heat transfer and friction factor correlations for double pipe heat exchanger with inner and outer corrugation. Energy Source, Part A: Recovery, Util Environ Eff. 2023;45(1):18–45.
77. Firoozeh ST, Pourmahmoud N, Khalilian M. Two-tube heat exchanger with variable groove angle on the inner pipe surface: experimental study. Appl Therm Eng. 2023;234:121274.
78. Ashraf G, Bilal S, Ishaq M, Saifullah SK, Alqahtani A, Malik M. Thermodynamic optimization in laminar and fully developed flow in double pipe heat exchanger with arrow-shaped extended surfaces: a novel design. Case Stud Therm Eng. 2024;54:103947.
79. Sharaf MA, Marzouk S, Aljabr A, Almehmadi FA, Kaood A, Alqaed S. Heat transfer enhancement in a double-pipe helical heat exchanger using spring wire insert and nanofluid. J Therm Anal Calorim. 2024. https://doi.org/10.1007/s10973-024-12992-1.
80. Jawarneh AM, Al-Widyan M, Al-Mashhadani Z. Experimental study on heat transfer augmentation in a double pipe heat exchanger utilizing jet vortex flow. Heat Transf. 2023;52(1):317–32.
81. Li J, Hou S, Teng D, Shen G. Experimental research on enhanced heat transfer of double-pipe exchanger with audible acoustic field. Int J Heat Mass Transf. 2023;201:123565.
82. Hedeshi M, Jalali A, Arabkoohsar A, Amiri Delouei A. Nanofluid as the working fluid of an ultrasonic-assisted double-pipe counter-flow heat exchanger. J Therm Anal Calorim. 2023;148(16):8579–91.
83. Sharaf MA, Marzouk S, Aljabr A, Almehmadi FA, Alam T, Teklemariyem DA. Effects of multi-spring wires on hydrothermal performance of double tube heat exchanger. Case Stud Therm Eng. 2024;60:104689.
84. Dhumal GS, Havaldar SN. Enhancing heat transfer performance in a double tube heat exchanger: experimental study with twisted and helical tapes. Case Stud Therm Eng. 2023;51:103613.
85. Chaurasia SR, Sarviya R. Experimental thermal performance analysis of fluid flow in a heat exchanger pipe with novel

double strip helical screw tape inserts for utilization of energy resources. Energy Sources Part A Recover Util Environ Eff. 2023;45(2):4268–81.
86. Dandoutiya BK, Kumar A. Study of thermal performance of double pipe heat exchanger using W-cut twisted tape. Energy Sources Part A Recover Util Environ Eff. 2023;45(2):5221–38.
87. Ali MA, Shehab SN. Numerical analysis of heat convection through a double-pipe heat exchanger: dimpled influence. J Eng Res. 2023;11(1):100016.
88. Zhang Y, Hangi M, Wang X, Rahbari A. A comparative evaluation of double-pipe heat exchangers with enhanced mixing. Appl Therm Eng. 2023;230:120793.
89. Hasan MF, Danışmaz M, Majel BM. Thermal performance investigation of double pipe heat exchanger embedded with extended surfaces using nanofluid technique as enhancement. Case Stud Therm Eng. 2023;43:102774.
90. Izadi M, Alshehri HM, Hosseinzadeh F, Rad MS, Hamida MBB. Numerical study on forced convection heat transfer of TiO2/water nanofluid flow inside a double-pipe heat exchanger with spindle-shaped turbulators. Eng Anal Boundary Elem. 2023;150:612–23.
91. Azizi Y, Bahramkhoo M, Kazemi A. Influence of non-uniform magnetic field on the thermal efficiency hydrodynamic characteristics of nanofluid in double pipe heat exchanger. Sci Rep. 2023;13(1):407.